

Tuning the Intramolecular Charge Transfer Emission from Deep Blue to Green in Ambipolar Systems Based on Dibenzothiophene S,S-Dioxide by Manipulation of Conjugation and Strength of the Electron Donor Units

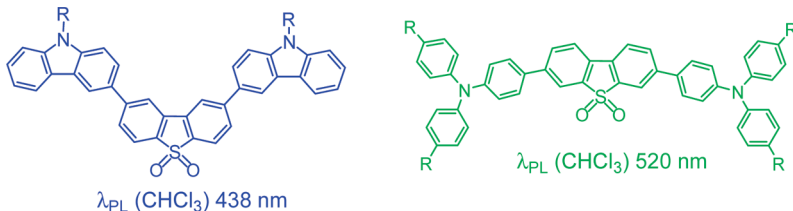
Kathryn C. Moss,[†] Konstantinos N. Bourdakos,[‡] Vandana Bhalla,^{†,§} Kiran T. Kamtekar,[†] Martin R. Bryce,^{*,†} Mark A. Fox,[†] Helen L. Vaughan,[‡] Fernando B. Dias,[‡] and Andrew P. Monkman[‡]

[†]Department of Chemistry, Durham University, Durham, DH1 3LE, U.K., and

[‡]Department of Physics, Durham University, Durham DH1 3LE, U.K., [§]Department of Chemistry, Guru Nanak Dev University, Amritsar-143005, India, and [†]Zumtobel LED Division, Green Lane Industrial Estate, Spennymoor DL16 6HL, U.K.

m.r.bryce@durham.ac.uk

Received May 7, 2010



The efficient synthesis and photophysical properties of a series of ambipolar donor–acceptor–donor systems is described where the acceptor is dibenzothiophene S,S-dioxide and the donor is fluorene, carbazole, or arylamine. The systems exhibit intramolecular charge transfer (ICT) states (of variable ICT character strengths) leading to fluorescence emission ranging from deep blue to green with moderate to high photoluminescence quantum yields. The emission properties can be effectively tuned by systematically changing the position of substitution on both donor and acceptor units (which affects the extent of conjugation) and the redox potentials of the donor units. The results are supported by cyclic voltammetric data and TD-DFT calculations.

Introduction

The development of conjugated organic materials for optoelectronic devices remains a key objective across many disciplines of science.¹ These materials have applications in organic/polymeric light-emitting diodes (O/PLEDs),² organic photovoltaics

(OPVs),³ organic field-effect transistors (OFETs),⁴ electrochromism,⁵ and sensors.⁶ Studies on π -conjugated oligomers provide valuable insights into relevant fundamental properties.⁷

The covalent combination of electron donor and electron acceptor units has provided a wealth of information about energy and charge transfer processes.⁸ For example, the luminescence of 9,9-dialkylfluorene copolymers⁹ can be tuned over a large wavelength range by utilizing intramolecular

(1) (a) Forrest, S. R.; Thompson, M. E. *Chem. Rev.* **2007**, *107*, 923–925. (Special Issue on Organic Electronics). (b) *Handbook of Conducting Polymers*, 3rd ed.; Skotheim, T. A., Reynolds, J. R., Eds.; CRC Press: New York, 2005.

(2) (a) Grimsdale, A. C.; Chan, K. L.; Martin, R. E.; Jokisz, P. G.; Holmes, A. B. *Chem. Rev.* **2009**, *109*, 897–1091. (b) *Organic Electroluminescence*; Kakafi, Z. H., Ed.; CRC Press: New York, 2005.

(3) (a) Martín, N.; Sánchez, L.; Herranz, M. A.; Illescas, B.; Guldi, D. *Acc. Chem. Res.* **2007**, *40*, 1015–1024. (b) Hermans, P.; Cheyns, D.; Rand, B. P. *Acc. Chem. Res.* **2009**, *42*, 1740–1747. (c) Cheng, Y.-J.; Yang, S.-H.; Hsu, C.-S. *Chem. Rev.* **2009**, *109*, 5868–5923.

(4) Katz, H. E.; Huang, J. *Annu. Rev. Mater. Res.* **2009**, *39*, 71–92.

(5) (a) Beaujuge, P. M.; Reynolds, J. R. *Chem. Rev.* **2010**, *110*, 268–320. (b) Sonmez, G.; Shen, C. K. F.; Rubin, Y.; Wudl, F. *Angew. Chem., Int. Ed.* **2004**, *43*, 1498–1502.

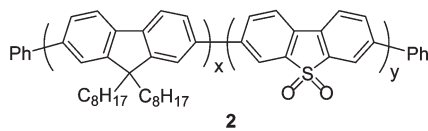
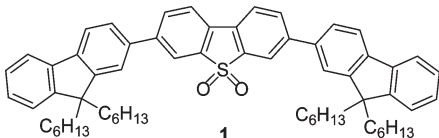
(6) Thomas, S. W., III; Joly, G. D.; Swager, T. M. *Chem. Rev.* **2007**, *107*, 1339–1386.

(7) (a) *Electronic Materials: The Oligomer Approach*; Müllen, K., Wegner, G., Eds.; Wiley-VCH: Weinheim, Germany, 1998. (b) Martin, R. E.; Diederich, F. *Angew. Chem. Int. Ed.* **1999**, *38*, 1350–1377. (c) Segura, J. L.; Martin, N. *J. Mater. Chem.* **2000**, *10*, 2403–2435.

(8) Laquai, F.; Park, Y.-S.; Kim, J.-J.; Bashé, T. *Macromol. Rapid Commun.* **2009**, *30*, 1203–1231.

(9) (a) Wallace, J. U.; Chen, S. H. In *Polyfluorenes*; Springer-Verlag: Berlin, 2008; Vol. 212, pp 145–186. (b) U. Scherf, U.; List, E. J. W. *Adv. Mater.* **2002**, *7*, 477–487. (c) Leclerc, M. *J. Polym. Sci., Part A: Polym. Chem.* **2001**, *39*, 2867–2873.

CHART 1



charge and energy transfer processes both in solution and in the solid state.¹⁰ Oligo-/polycarbazoles are also a benchmark family of materials which are widely used for O/PLEDs, OFETs, and OPVs.¹¹ They are predominantly hole transporters (p type) with reversible redox properties, strong luminescence, and a larger band gap than for polyfluorenes. Similarly, arylamines are well documented, mainly due to their high hole-transporting ability.¹² Many optoelectronic applications require ambipolar compounds: i.e., those able to accept, transport, or store both holes and electrons.^{13–15} Intramolecular charge transfer (ICT) processes¹⁶ often play an important role in the photophysics of ambipolar systems. For example, Kulkarni et al. demonstrated an increase in ICT emission upon increasing the strength of the donor unit, comparing *N*-methylcarbazole with the stronger donor *N*-methylphenothiazine in acceptor–donor–acceptor trimers (acceptor = phenylquinoline).¹⁷ Estrada and Neckers studied fluorene-9-ylidene malononitrile derivatives as strong acceptors, linked through the 2,7- or 3,6-positions via alkyne bridges to carbazole donors to provide donor–acceptor–donor triads.¹⁸ Effective electronic communication

(10) (a) Beaupré, S.; Leclerc, M. *Adv. Funct. Mater.* **2002**, *12*, 192–196. (b) Yang, R.; Tian, R.; Yan, J.; Zhang, Y.; Yang, J.; Hou, Q.; Yang, W.; Zhang, C.; Cao, Y. *Macromolecules* **2005**, *38*, 244–253. (c) Wu, W.-C.; Liu, C.-L.; Chen, W.-C. *Polymer* **2006**, *47*, 527–538. (d) Zhu, Y.; Gibbons, K. M.; Kulkarni, A. P.; Jenekhe, S. A. *Macromolecules* **2007**, *40*, 804–813. (e) Kulkarni, A. P.; Zhu, Y.; Jenekhe, S. A. *Macromolecules* **2008**, *41*, 339–345. (f) Wu, P.-T.; Kim, F. S.; Champion, R. D.; Jenekhe, S. A. *Macromolecules* **2008**, *41*, 7021–7028.

(11) (a) Beaupré, S.; Boudreault, P.-L. T.; Leclerc, M. *Adv. Mater.* **2010**, *22*, E6–E27. (b) Zhao, Z.; Xu, X.; Wang, H.; Lu, P.; Yu, G.; Liu, Y. *J. Org. Chem.* **2008**, *73*, 594–602. (c) Blouin, N.; Michaud, A.; Gendron, D.; Wakim, S.; Blair, E.; Neagu-Plesu, R.; Belletête, M.; Durocher, G.; Tao, Y.; Leclerc, M. *J. Am. Chem. Soc.* **2008**, *130*, 732–742. (d) Wakim, S.; Aich, B. R.; Tao, Y.; Leclerc, M. *Polym. Rev.* **2008**, *48*, 432–462. (e) Adhikari, R. M.; Mondal, R.; Shah, B. K.; Neckers, D. C. *J. Org. Chem.* **2007**, *72*, 4727–4732. (f) Blouin, N.; Michaud, A.; Leclerc, M. *Adv. Mater.* **2007**, *19*, 2295–2300. (g) Grigalevicius, S.; Ma, L.; Xie, Z.; Scherf, U. *J. Polym. Sci., Part A: Polym. Chem.* **2006**, *44*, 5987–5994. (h) Sonntag, M.; Kreger, K.; Hanft, D.; Strohriegel, P.; Setayesh, S.; de Leeuw, D. *Chem. Mater.* **2005**, *17*, 3031–3039. (i) Morin, J.-F.; Drolet, N.; Tao, Y.; Leclerc, M. *Chem. Mater.* **2004**, *16*, 4619–4626. (j) Thomas, K. R. J.; Liu, J. T.; Tao, Y.-T.; Chuen, C.-H. *J. Mater. Chem.* **2002**, *12*, 3516–3522.

(12) (a) Shirota, Y. *J. Mater. Chem.* **2000**, *10*, 1–25. (b) Jungermann, S.; Riegel, N.; Muller, D.; Meerholz, K.; Nuyken, O. *Macromolecules* **2006**, *39*, 8911–8919. (c) Kondakov, D. Y. *J. Appl. Phys.* **2008**, *104*, 084520.

(13) (a) Shirota, Y.; Kageyama, H. *Chem. Rev.* **2007**, *107*, 953–1010. (b) Zaumseil, J.; Sirringhaus, H. *Chem. Rev.* **2007**, *107*, 1296–1323.

(14) Reviews of electron-transporting materials: (a) Hughes, G.; Bryce, M. R. *J. Mater. Chem.* **2005**, *15*, 94–107. (b) Kulkarni, A. P.; Tonzola, C. J.; Babel, A.; Jenekhe, S. A. *Chem. Mater.* **2004**, *16*, 4556–4573.

(15) (a) Geramita, K.; McBee, J.; Tilley, T. D. *J. Org. Chem.* **2009**, *74*, 820–829. (b) Geramita, K.; Tao, Y.; Segalman, R. A.; Tilley, T. D. *J. Org. Chem.* **2010**, *75*, 1871–1887.

(16) (a) Grabowski, Z. R.; Rotkiewicz, K.; Rettig, W. *W. Chem. Rev.* **2003**, *103*, 3899–4031. (b) Gómez, I.; Reguero, M.; Boggio-Pasqua, M.; Robb, M. A. *J. Am. Chem. Soc.* **2005**, *127*, 7119–7129. (c) Mallick, A.; Maiti, S.; Haldar, B.; Purkayastha, P.; Chattopadhyay, N. *Chem. Phys. Lett.* **2003**, *371*, 688–693. (d) Paul, B. K.; Samanta, A.; Kar, S.; Guchhait, N. *J. Lumin. J. Photochem. Photobiol. C* **2007**, *8*, 109–127. (f) Mahanta, S.; Singh, R. B.; Kar, S.; Guchhait, N. *J. Photochem. Photobiol. A* **2008**, *194*, 318–326. (g) Chakraborty, A.; Kar, S.; Nath, D. N.; Guchhait, N. *J. Phys. Chem. A* **2006**, *110*, 12089–12095.

(17) Kulkarni, A. P.; Kong, X. X.; Jenekhe, S. A. *Adv. Funct. Mater.* **2006**, *16*, 1057–1066.

(18) Estrada, L. A.; Neckers, D. C. *J. Org. Chem.* **2009**, *74*, 8484–8487.

was observed through the 3,6-positions to the fluorene-9-ylidene malononitrile core. However, in contrast with the donor–acceptor–donor systems described in the present article, the ICT state in these fluorene-9-ylidene malononitrile derivatives was a nonradiative deactivation pathway (i.e., nonemissive), with one of the 3,6-disubstituted oligomers showing total emission quenching in polar solvents.¹⁸

Our group¹⁹ and other workers²⁰ have incorporated dibenzothiophene *S,S*-dioxide (**S**) as an electron-deficient comonomer unit in oligo-/polyfluorene (**F**) backbones, e.g. trimer **1**^{19a} and polymer **2**^{19d} (Chart 1), which show high luminescence efficiency. DFT calculations and cyclic voltammetric data established that the lower energy LUMO levels of the sulfone unit enhance the electron-accepting properties of **1** and **2**.

In solution, **F–S** co-oligomers and copolymers of type **1** and **2** show a degree of intramolecular charge transfer (ICT) character and excited state relaxation depending on the nature of the local environment; e.g. the solvent polarity.^{19b,c} In nonpolar solvents, such as hexane or toluene, a well-structured emission is observed, in agreement with minimal conformation and solvent relaxations following excitation, whereas in polar solvents, such as acetonitrile, ethanol, and chloroform, broad, featureless (and red-shifted) ICT emission is dominant. The stability of the ICT state in **F–S** co-oligomers and copolymers is reduced by more twisted backbone conformations enforced by substituent effects on the **S** units.²¹ Ambipolar molecules comprising disubstituted **S** units as the acceptor moiety and diphenylamine/triphenylamine donor moieties have also been studied.²²

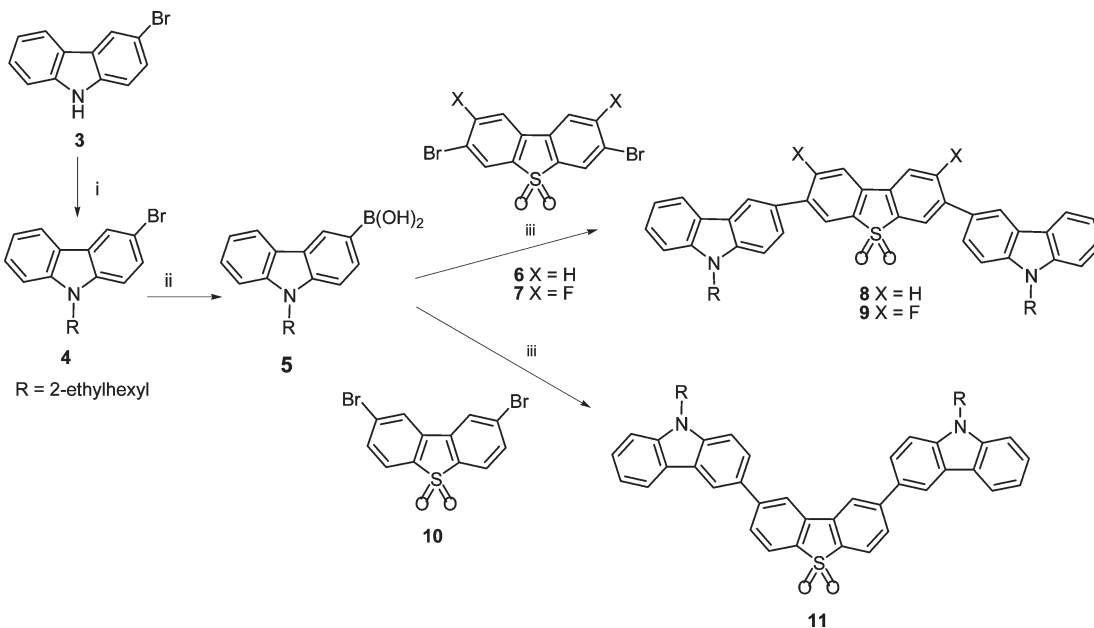
The present work describes new ambipolar oligomers containing **S** as the core unit. The objective is to tune the emission properties by combining the strategies of conjugation control (by systematically changing the substitution pattern between donor and acceptor) and varying the redox potential of the donor unit: namely, carbazole (**Cz**), di-/triphenylamine (**DPA**, **TPA**), and fluorene (**F**).

(19) (a) Perepichka, I. I.; Perepichka, I. F.; Bryce, M. R.; Palsson, L. O. *Chem. Commun.* **2005**, 3397–3399. (b) Dias, F. B.; Pollock, S.; Hedley, G.; Palsson, L.-O.; Monkman, A.; Perepichka, I. I.; Perepichka, I. F.; Tavasli, M.; Bryce, M. R. *J. Phys. Chem. B* **2006**, *110*, 19329–19339. (c) Dias, F. B.; King, S.; Monkman, A. P.; Perepichka, I. I.; Kryuchkov, M. A.; Perepichka, I. F.; Bryce, M. R. *J. Phys. Chem. B* **2008**, *112*, 6557–6566. (d) King, S. M.; Perepichka, I. I.; Perepichka, I. F.; Dias, F. B.; Bryce, M. R.; Monkman, A. P. *Adv. Funct. Mater.* **2009**, *19*, 586–591. (e) Dias, F. B.; Kamtekar, K. T.; Cazati, T.; Williams, G.; Bryce, M. R.; Monkman, A. P. *ChemPhysChem* **2009**, *10*, 2096–2104.

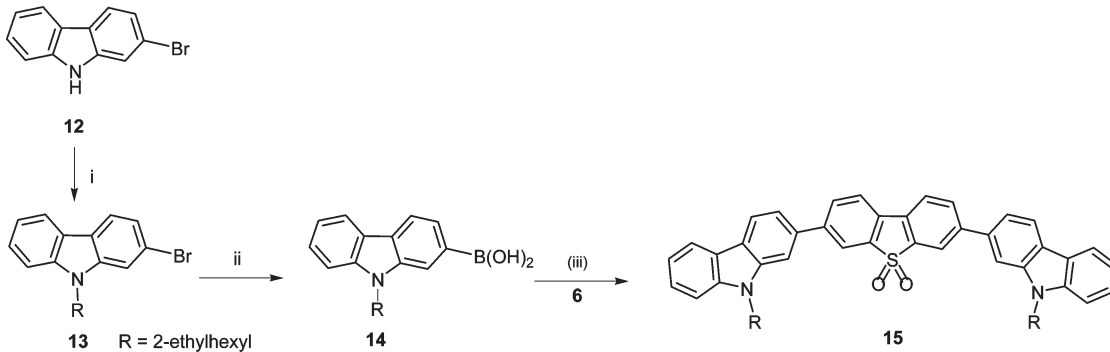
(20) (a) Yang, F.; Sun, K.; Cao, Z. J.; Li, Z. H.; Wong, M. S. *Synth. Met.* **2008**, *158*, 391–395. (b) Liu, H.; Zou, J. H.; Yang, W.; Wu, H. B.; Li, C.; Zhang, B.; Peng, J. B.; Cao, Y. *Chem. Mater.* **2008**, *20*, 4499–4506. (c) Li, Y. Y.; Wu, H. B.; Zou, J. H.; Ying, L.; Yang, W.; Cao, Y. *Org. Electron.* **2009**, *10*, 901–909.

(21) (a) Liu, J.; Hu, S.; Zhao, W.; Zou, Q.; Luo, W.; Yang, W.; Peng, J.; Cao, Y. *Macromol. Rapid Commun.* **2010**, *31*, 496–501. (b) Kamtekar, K. T.; Vaughan, H. L.; Lyons, B. P.; Monkman, A. P.; Pandya, S. U.; Bryce, M. R. *Macromolecules* **2010**, *43*, 4481–4488. (c) Li, H.; Batsanov, A. S.; Moss, K. C.; Vaughan, H. L.; Dias, F. B.; Kamtekar, K. T.; Bryce, M. R.; Monkman, A. P. *Chem. Commun.* **2010**, *46*, 4812–4814.

(22) Huang, T. H.; Lin, J. T.; Chen, L. Y.; Lin, Y. T.; Wu, C. C. *Adv. Mater.* **2006**, *18*, 602–606.

SCHEME 1. Synthesis of **8**, **9**, and **11**^a

^aReagents and conditions: (i) 2-ethylhexyl bromide, KO'Bu, DMF, 130 °C, 55%; (ii) "BuLi, (iPrO)₃B, concentrated HCl, THF, -78 to 20 °C, 51%; (iii) Pd(PPh₃)₂Cl₂, K₂CO₃ (aq), 1,4-dioxane, 110 °C, 78% for **8**, 50% for **9**, 78% for **11**.

SCHEME 2. Synthesis of **15**^a

^aReagents and conditions: (i) 2-ethylhexyl bromide, KO'Bu, DMF, 130 °C, 80%; (ii) "BuLi, (iPrO)₃B, concentrated HCl, THF, -78 to 20 °C, 67%; (iii) **6**, Pd(PPh₃)₂Cl₂, K₂CO₃ (aq), 1,4-dioxane, 110 °C, 78%.

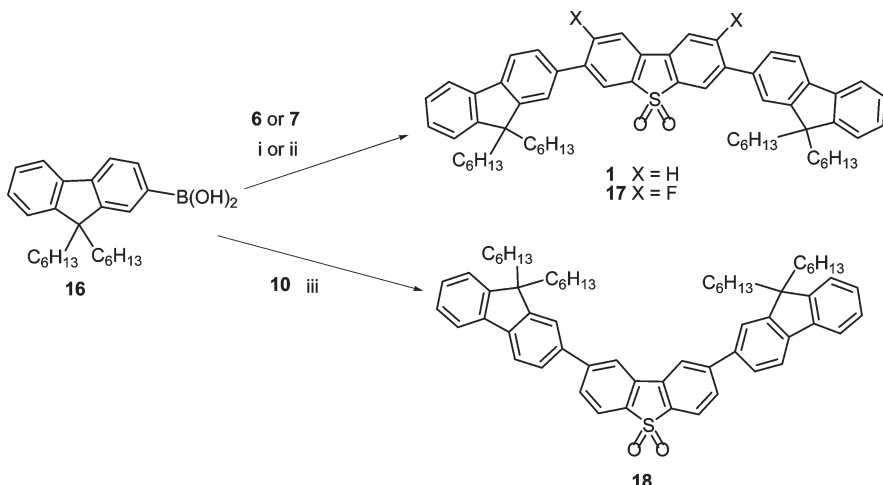
Results and Discussion

A series of **Cz–S–Cz** trimers, as well as their analogous **F–S–F** trimers, were synthesized via palladium-catalyzed Suzuki–Miyaura coupling reactions (Schemes 1–3). The 3,7-dibromo- (linear) and 2,8-dibromo-substituted (bent) S units **6**,^{19a} **7**,^{21c} and **10**^{20b} were synthesized according to previously reported procedures. The carbazole boronic acid derivatives **5** and **14** were synthesized in good yields from **4** and **13**, respectively, by a sequence of lithiation, borylation, and hydrolysis. The 2-ethylhexyl substituent was chosen to enhance solubility. For the cross-couplings dichlorobis(triphenylphosphine)palladium(II) or tetrakis(triphenylphosphine)palladium(0) was used as a catalyst and trimers **8**, **9**, **11**, **15**, **17**, and **18** were obtained in moderate to good yields as either white or yellow solids. N-substituted carbazole trimers **20** and **21** were synthesized via palladium-catalyzed C–N cross-coupling reactions of carbazole **19** with **6** and **10**, respectively (Scheme 4). The very low solubility of **20** and **21** made reaction and workup difficult, and the

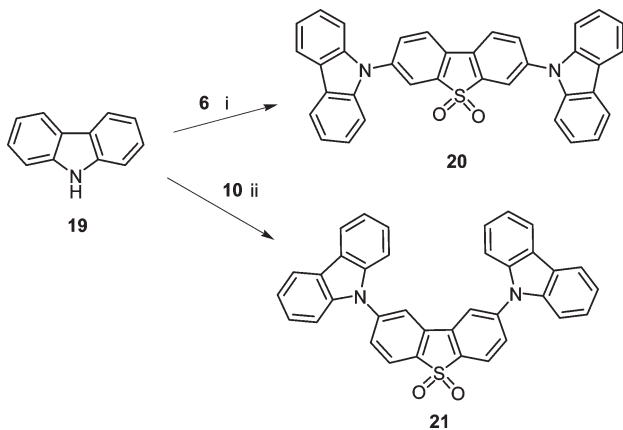
products were obtained in low yields. The diarylamine analogue **23** was similarly synthesized from **6**. The triarylamine analogue **26** was synthesized by a different route. The diboronic ester derivative **24** underwent Suzuki cross-coupling (Scheme 5) with **25** to give **26**. Both **23** and **26** are bright yellow solids with good solubility imparted by the *n*-butyl substituents.

Cyclic voltammetric data on all the **Cz–S–Cz**, **DPA–S–DPA**, **TPA–S–TPA**, and **F–S–F** trimers synthesized here are given in Table 1. The carbazolyl derivatives show irreversible oxidation waves at ca. 0.8–1.0 V typically found for carbazoles.²³ These potentials are lower than those of the reversible oxidation waves observed at ca. 1.2–1.4 V for the fluorenyl analogues. Even lower oxidation potentials at ca. 0.4 V were obtained for the DPA (**23**) and TPA compounds (**26**), demonstrating a decrease in oxidation potential with an

(23) Brunner, K.; van Dijken, A.; Börner, H.; Bastiaansen, J. J. A. M.; Kiggen, N. M. M.; Langeveld, B. M. W. *J. Am. Chem. Soc.* **2004**, *126*, 6035–6042.

SCHEME 3. Synthesis of **1**, **17**, and **18**^a

^aReagents and conditions: (i) **6**, Pd(PPh₃)₂Cl₂, K₂CO₃ (aq), 1,4-dioxane, 110 °C, 86% for **1**; (ii) **7**, Pd(PPh₃)₄, Na₂CO₃ (aq), toluene, 110 °C, 50% for **17**; (iii) **10**, Pd(PPh₃)₂Cl₂, K₂CO₃ (aq), 1,4-dioxane, 110 °C, 21%.

SCHEME 4. Synthesis of **20** and **21**^a

^aReagents and conditions: (i) **6**, Pd₂(dba)₃, xphos, NaO*Bu*, *Bu*OH, toluene, 110 °C, 24%; (ii) **10**, Pd₂(dba)₃, *Bu*₃PHBF₄, *Bu*OH, toluene, 110 °C, 20%.

increase in donor strength (fluorene → carbazole → arylamine). While trimer **26** showed a reversible two-electron oxidation wave, indicating that oxidizing one amine group has little influence on the oxidation of the second amine group, trimer **23** showed two well-separated one-electron reversible waves ($\Delta E = 300$ mV), implying that oxidation at one amine group strongly influences the oxidation of the second amine group. These waves suggest that substantial conjugation exists across the linear S unit. The reduction potentials observed for the reversible waves of these trimers are within the range of ca. -1.9 to -2.4 V and arise from the one-electron reduction of the S unit in all cases. The difluorinated trimers **9** and **17** are more easily reduced by ca. 0.1–0.3 V in comparison to their parent analogues **8** and **1**, respectively. These data illustrate the ambipolar nature of these compounds.

The photophysical data for the trimers are summarized in Table 2. There is a progressive red shift in the absorption and emission in the series fluorene → carbazole → arylamine, in line with the increasing electron-donating ability of these

substituents: e.g., λ_{PL} (CHCl₃) **1** at 427 nm, 2.90 eV, **8** at 458 nm, 2.71 eV, and **26** at 520 nm, 2.38 eV (Figure 1). This trend corresponds with the HOMO–LUMO gaps of 3.37 eV for **1**, 3.06 eV for **8**, and 2.65 eV for **26** determined by cyclic voltammetric studies (Table 1). Thus, the fluorene-containing trimers exhibit deep blue fluorescence which becomes sky blue for the carbazole analogues and green for the arylamine analogues (see Figure SI2-8 in the Supporting Information for a photograph showing the emission colors of compounds **1**, **8**, and **23**). The TPA-based trimer **26** emits at the longest wavelength of all the compounds in this study (in both toluene and chloroform), consistent with the stronger donor enhancing the red shift.

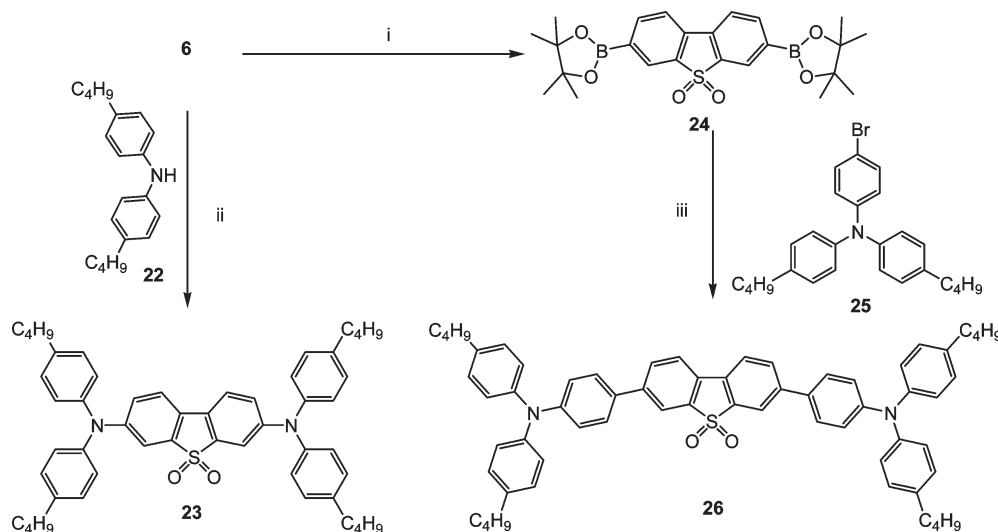
All the oligomers show positive solvatochromism in their photoluminescence (PL) spectra due to ICT behavior, which enables the emission color to be tuned by varying the solvent polarity. Table 2 shows the absorption and emission data in both toluene and chloroform for all compounds. Compounds **20** and **21** are distinct in that they are bonded directly through the carbazole N atom rather than via one of the ring carbons and are considerably less soluble than the other trimers discussed here.

Table 3 gives the Stokes and solvatochromic shift energies. There appear to be two distinct groups in this study based on the ICT character of these trimers. Trimmers with relatively strong ICT may be defined by

- (i) a lack of fine structure emission in toluene (only one band value given in Table 2)
- (ii) a large positive solvatochromic shift in the emission band on changing from toluene to chloroform (>1000 cm⁻¹ in Table 3)
- (iii) a significantly positive solvatochromatic shift in the low-energy absorption maximum from toluene to chloroform (>400 cm⁻¹ in Table 3)
- (iv) larger Stokes shifts (5000–6000 cm⁻¹) in both toluene and chloroform

Trimmers with relatively weak ICT character may, therefore, be defined by

- (i) the presence of fine structure emission in toluene (two band values given in Table 2)

SCHEME 5. Synthesis of 23 and 26^a

^aReagents and conditions: (i) $\text{B}_2(\text{pin})_2$, $\text{Pd}(\text{dppf})_2\text{Cl}_2$, KOAc , DMF , 90°C , 26%; (ii) $\text{Pd}_2(\text{dba})_3$, $t\text{Bu}_3\text{PHBF}_4$, $\text{NaO}'\text{Bu}$, toluene , 107°C , 44%; (iii) $\text{Pd}(\text{PPh}_3)_2\text{Cl}_2$, K_2CO_3 (aq), toluene , 110°C , 33%.

TABLE 1. Electrochemical Data and Computed Frontier Orbital Energies

compd	donor	acceptor	E_{ox} (V) ^{a,b}	E_{red} (V) ^a	HLG (CV) (eV) ^f	HOMO (calcd) (eV) ^g	LUMO (calcd) (eV) ^g	HLG (calcd) (eV) ^h
1	F	linear	1.20	-2.17	3.37	1.06	-2.57	3.63
8	3-Cz	linear	0.83 ^c	-2.23	3.06	0.73	-2.86	3.59
9	3-Cz	linear, F_2	1.04 ^c	-2.14	3.18	0.84	-2.61	3.45
11	3-Cz	bent	0.75 ^c	-2.22	2.97	0.93	-2.90	3.83
15	2-Cz	linear	0.81 ^{c,d}	-2.13	2.94	0.98	-2.63	3.61
17	F	linear, F_2	1.39	-1.91	3.30	1.18	-2.65	3.52
18	F	bent	1.24	-2.26	3.50	1.28	-2.65	3.93
20	N-Cz	linear	0.96 ^{c,d}	-2.18	3.14	1.00	-2.42	3.42
21	N-Cz	bent	0.94 ^{c,d}	-2.19	3.13	1.16	-2.41	3.57
23	DPA	linear	0.40 ^e	-2.39	2.79	0.24	-3.13	3.37
26	TPA	linear	0.45	-2.20	2.65	0.31	-2.78	3.09

^a $E_{1/2}$ values reported with reference to the ferrocene/ferrocenium couple at 0.00 V using tetrabutylammonium hexafluorophosphate (0.2 M) in DCM as electrolyte solution. ^bPoorly defined oxidation wave arising from two simultaneous one-electron-oxidation processes in most cases. ^cIrreversible wave; $E_{1/2}$ values estimated from deconvolution data. ^dIrreversible reduction wave at ca. -2.0 V observed after oxidation. ^eWell-defined one-electron reversible wave with a second reversible wave at 0.70 V. ^fHOMO–LUMO gap derived from the difference between oxidation and reduction potentials. ^gCalculated HOMO/LUMO values converted to the ferrocene/ferrocenium couple: $E = -4.8 \text{ V} - E(\text{HOMO/LUMO}) \text{ V}$. ^hCalculated HOMO–LUMO gap.

- (ii) a small positive solvatochromic shift in the emission band on changing from toluene to chloroform (< 1000 cm^{-1} in Table 3)
- (iii) little solvatochromatic shift in the low-energy absorption maximum from toluene to chloroform (< 400 cm^{-1} in Table 3)
- (iv) smaller Stokes shifts (3000–4000 cm^{-1}) in both solvents

Compounds with strong CT character are the 2,8-disubstituted bent trimers **11**, **18**, and **21**, whereas those with weaker CT character are the 3,7-disubstituted linear trimers **1**, **8**, **9**, **15**, **17**, and **20**. The linear compounds containing DPA and TPA units (**23** and **26**, respectively) are between. The CT strength may be measured by comparing the emission peak maxima in different solvents: compound **11** represents strong ICT character, whereas the previously reported compound **1** is representative of weak ICT character (for details of the solvatochromism of **1** see ref 19b). Solvatochromic effects were studied in detail for compound **11**, and Figure 2 shows the emission spectra in eight solvents of different polarities (see Figure SI2-19 for the corresponding absorption spectra). Figure 3 depicts the emission colors of **11** in four solvents.

For compound **11** spectral shifts due to solvent polarity are seen in both the absorption and emission spectra, with a profound effect seen in the emission. The emission spectra are red-shifted and broadened as the solvent polarity increases (from MCH to methanol), typical of ICT excited states.^{24,25} The vibronic structure of the emission spectrum can be seen in MCH but disappears as the solvent polarity increases, again indicative of an excited ICT state.²⁶

By plotting the wavelengths of the emission maxima of **11** in the different solvents as a function of the solvent orientation polarizability, $\Delta f = (\epsilon - 1)/(2\epsilon + 1) - 1/2((n^2 - 1)/(2n^2 + 1))$ (Lippert–Mataga equation),^{19b} the corresponding Lippert plot is obtained (Figure 4). It can be seen from this plot that the spectral shift of the emission follows (to a good approximation) a linear trend. Polar aprotic solvents such as dichloromethane and acetonitrile which are included in this plot indicate that the spectral shift is the result of solvent polarity and is not due to

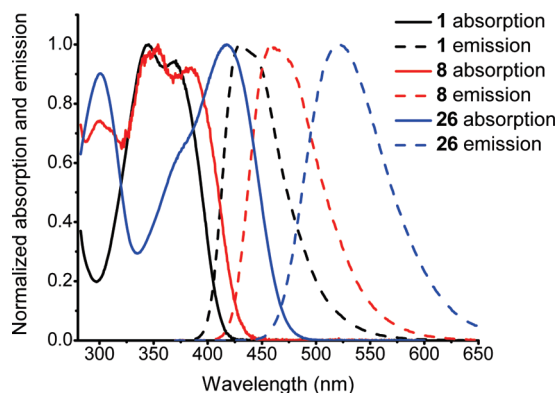
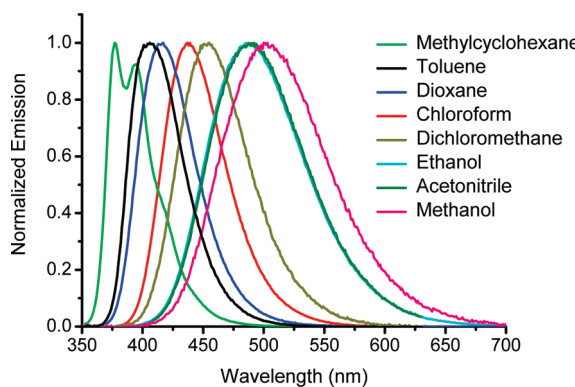
(24) Diwu, Z.; Lu, Y.; Zhang, C.; Klaubert, D. H.; Haugland *Photochem. Photobiol.* **1997**, *66*, 424–431.

(25) Rettig, W. *Angew. Chem., Int. Ed. Engl.* **1986**, *25*, 971–988.

(26) Lakowicz, J. R., Ed. *Principles of Fluorescence Spectroscopy*, 2nd ed.; Kluwer Academic/Plenum Publishers: New York, 1999.

TABLE 2. Photophysical Properties

compd	λ_{abs} (nm), toluene	ϵ ($M^{-1} \text{cm}^{-1}$), toluene	λ_{abs} (nm), chloroform	λ_{PL} (nm), toluene	λ_{PL} (nm), chloroform	Φ_{PL}^a , toluene	λ_{ex} (nm) for Φ_{PL}
1	344 366	55 800 57 100	352 367	412 ^b 433	427 ^b 440	0.90 ± 0.10	380
8	355 379	35 900 34 900	355 382	433 ^b 450	458	0.45 ± 0.05	380
9	352 ^c 377	30 700 36 300	357 ^c 387	432 ^b 450	454	0.58 ± 0.05	380
11	299 340	62 800 27 000	300 355	408	438	0.25 ± 0.10	360
15	339 370	38 800 53 000	339 371	420 ^b 440	438	0.55 ± 0.05	380
17	360	49 100	362	411 ^b 429	425 ^b 440	1.00 ± 0.10	380
18	300 320	47 000 43 700	300 326	377 387 ^b	409	0.59 ± 0.05	320
20	338 379	18 850 14 760	350 384	431 442 ^b	454	0.57 ± 0.05	380
21	323 336	13 000 16 500	322 334	424	456	0.26 ± 0.10	360
	351 ^b	9100	354 ^c				
23	298 380	20 600 33 600	296 380	482	516	0.60 ± 0.05	375
	428 ^b	13 440	436 ^c				
26	300 411	35 100 40 500	302 418	471	520	0.75 ± 0.05	375

^aPhotoluminescence quantum yield. ^bHighest maximum. ^cShoulder.**FIGURE 1.** Influence of the donor substituents on the absorption and emission spectra for the linear systems **1**, **8**, and **26** in chloroform.**FIGURE 2.** Emission spectra for **11** in solvents of different polarities.TABLE 3. Solvatochromic and Stokes Shift Energies (in cm^{-1}) for the Trimers

compd	solvatochromic		Stokes	
	$\Delta\lambda_{\text{abs}}$	$\Delta\lambda_{\text{PL}}$	$\lambda_{\text{abs}} - \lambda_{\text{PL}}$ (toluene)	$\lambda_{\text{abs}} - \lambda_{\text{PL}}$ (chloroform)
1	250	500	3450	3950
8	200	750	3800	4350
9	350	550	4000	4200
11	1250	1700	4900	5350
15	100	400	3750	4100
17	150	700	3950	4550
18	1050	1750	5550	6250
20	500	850	3650	4000
21^a	250	1650	4900	6300
23^a	450	1350	2600	3550
26	400	2000	3100	4700

^aTentative low-energy absorption value based on a shoulder.hydrogen bonding. Figure 4 also shows the Lippert plot of **1** for comparison (data taken from ref 19b). The slope of the Lippert

plots of both **1** and **11** suggests, as can be seen from the Lippert–Mataga equation, that the excited-state dipole moment is larger than the ground-state dipole moment, which is also confirmed by the transient spectral shift to lower energies, observed in polar media from time-resolved data (as discussed in ref 19b). Especially for **11** the slope is much steeper, which, assuming that the cavity radii are similar for both compounds, yields a much larger difference between the dipole moments of the excited and ground states. This suggests a large charge separation for **11** in the excited state, which is also compatible with the frontier orbital picture obtained through DFT calculations (vide infra, Figure 8).

The assumption that both compounds have similar cavity radii is based on the fact that for both of them the longest axis is estimated to be ca. 25 Å and according to Lippert²⁷ the cavity radius for nonspherical molecules can be approximated to 40% of their longest axis.

(27) El-Gezawy, H.; Rettig, W.; Lapouyade, R. *J. Phys. Chem. A* 2006, 110, 67–75.

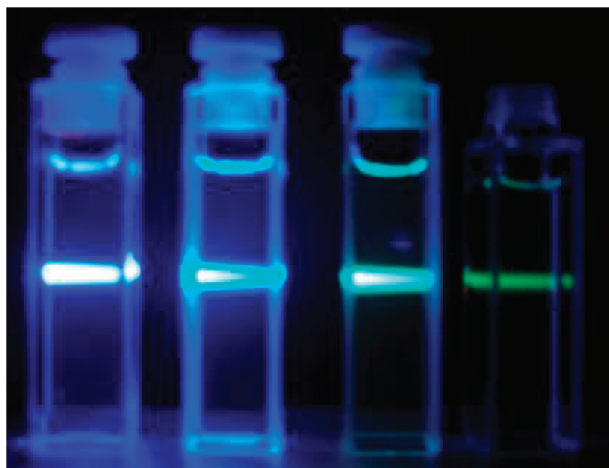


FIGURE 3. Photograph showing the effect of solvent polarity on the emission color of **11** when excited by a 360 nm laser with 2 ps pulses (MCH = methylcyclohexane): (left to right) MCH, CHCl_3 , EtOH, and MeOH.

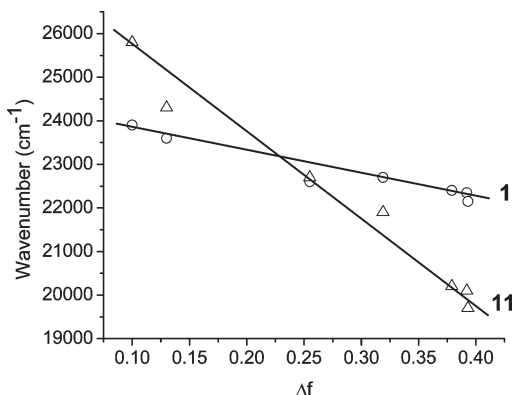


FIGURE 4. Lippert plots for **1** and **11**.

Changing the position of the donor substituents on the S unit significantly affects the absorption and emission spectra. For **11** (2,8-disubstitution: bent) compared to isomer **8** (3,7-disubstitution: linear), the emission is blue-shifted (Figure 5). This can be explained by extended conjugative (para) effects in **8** where four rings are in conjugation, whereas in **11** only two rings are in conjugation. This effect is also seen in the analogous F–S systems **1** and **18**. However, the bent vs linear effects of the *N*-carbazole groups on the emission maxima in **20** and **21** (Figure 6) are much smaller, implying that less conjugation is taking place between the carbazolyl groups and the S unit in the linear isomer.

Analogous 2,8-disubstituted (bent) S units with both DPA and TPA substituents (without butyl chains) have been previously reported;²² they exhibit blue-shifted emission in toluene compared with **23** and **26**, indicating similar bent vs linear effects. A similar effect was reported by Estrada and Neckers for trimers with the fluoren-9-ylidene malonitrile acceptor at the core: for the linear trimer the HOMO was delocalized, whereas for the bent isomer the HOMO was predominantly localized on the donor units.¹⁸

(28) Grisorio, R.; Melcarne, G.; Suranna, G. P.; Mastrolilli, P.; Nobile, C. F.; Cosma, P.; Fini, P.; Colella, S.; Fabiano, E.; Piacenza, M.; Sala, F. D.; Ciccarella, G.; Mazzeo, M.; Gigli, G. *J. Mater. Chem.* **2010**, *20*, 1012–1018.

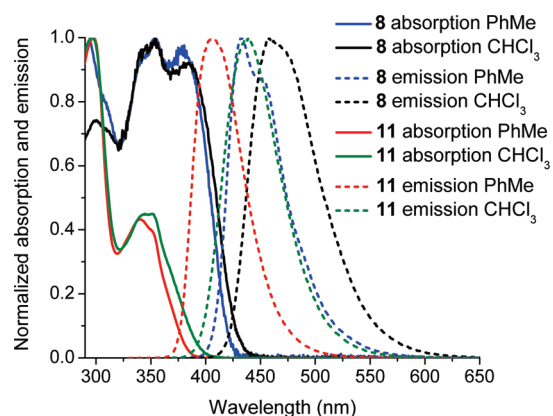


FIGURE 5. Absorption and emission spectra for **8** and **11**, representing linear vs bent trimers, showing solvent effects on the λ_{\max} values.

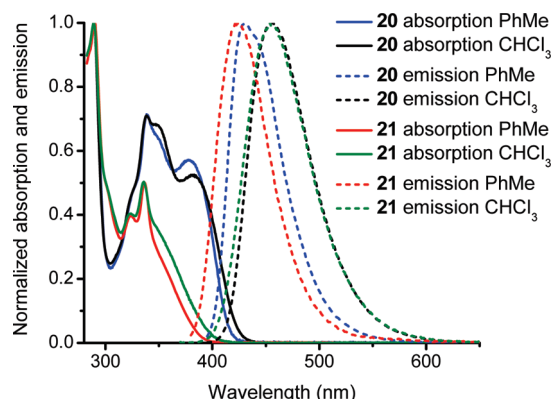


FIGURE 6. Absorption and emission spectra for **20** and **21** showing the solvent effects on the maxima values. Bent vs linear conformations have little effect on the emission maxima values.

As we were completing this paper, Grisorio et al. reported the *N*-methylcarbazole analogues of **8** and **11**.²⁸ Due to limited solubility they were unable to study the solvatochromism of these compounds, as we have done for **8** and **11**. Their observation that substitution of S in the 2,8-position gave more blue-shifted emission in chloroform due to a reduced conjugation effect, in comparison to the 3,7-isomer, is consistent with our data discussed above for **8** and **11**.

A general trend is that the bent systems have lower fluorescence quantum yields compared to their linear isomers: compare **1** and **18**, **8** and **11**, and **20** and **21** (i.e. linear versus bent, respectively). The addition of the fluorine substituents increases the quantum yields Φ_{PL} from 0.45 to 0.58 (± 0.05), on comparing **8** and **9** in toluene, presumably due to a decrease in nonradiative decay pathways caused by C–H bond vibrations.²⁹ A similar effect is observed for the analogous F–S systems **1** and **17**.^{21c}

All time-resolved fluorescence decays could be fitted with two exponential components whose amplitudes and time constants, are given in Table 4, along with the average lifetime, the values of excitation and collection wavelengths, the solvent, and the local χ^2 values of the fitting in each case. The average lifetime was calculated from the expression³⁰ $\tau_{av} = \sum_i A_i \tau_i^2 / \sum_i A_i \tau_i$, where A_i

(29) Babudri, F.; Farinola, G. M.; Naso, F.; Ragni, R. *Chem. Commun.* **2007**, 1003–1022.

(30) Lakowicz, J. R. *Principles of Fluorescence Spectroscopy*, 3rd ed.; Springer: Singapore, 2006.

and τ_i are the amplitude and time constant of each exponential, respectively, and τ_{av} is the average lifetime. For all toluene solutions, except for **1** (see the previous discussion for this compound),^{19c} both components have positive amplitudes with the fast components having time constants in the range of hundreds of picoseconds and the slower components having time constants in the range of nanoseconds.

The pre-exponential amplitude associated with the faster component is always small, and the weight of this decay

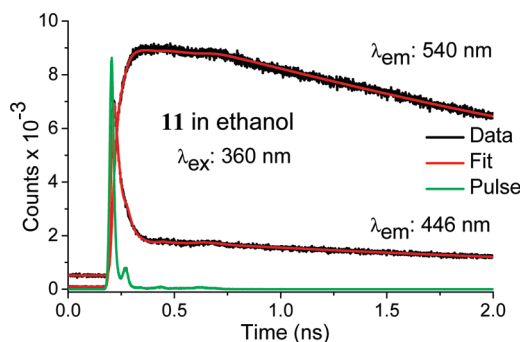


FIGURE 7. Fluorescence decays for **11** in ethanol collected at 446 and 540 nm.

TABLE 4. Lifetimes of Compounds

compd	solvent	λ_{exc} (nm)	λ_{em} (nm)	τ_2 (ns) (A_2)	τ_1 (ns) (A_1)	χ^2	τ_{av} (ns)
1^a	toluene	380	415	0.030 (-0.05)	1.08 (1.00)	1.12	1.08
8	toluene	360	433	0.173 (0.12)	1.47 (0.88)	1.05	1.45
9	toluene	360	431	0.153 (0.12)	1.27 (0.88)	1.25	1.25
11	toluene	377	489	0.098 (0.07)	1.13 (0.93)	1.04	1.12
	ethanol	360	446	0.028 (0.87)	3.98 (0.13)	1.12	3.79
	ethanol	360	540	0.023 (-0.84)	3.93 (1.00)	1.48	3.93
15	toluene	377	420	0.246 (0.09)	1.24 (0.91)	1.05	1.22
17	toluene	360	431	0.153 (0.11)	0.92 (0.89)	1.07	0.90
18	toluene	363	390	0.129 (0.07)	1.22 (0.93)	1.10	1.21
20	toluene	360	430	0.173 (0.18)	3.93 (0.82)	1.45	3.89
21	toluene	360	425	0.070 (0.13)	2.68 (0.86)	1.10	2.68
23	toluene	381	483	0.154 (0.04)	4.20 (0.25)	1.43	4.17
26	toluene	377	490	0.305 (0.07)	1.49 (0.93)	1.02	1.47

^aData for compound **1** are taken from ref 19c.

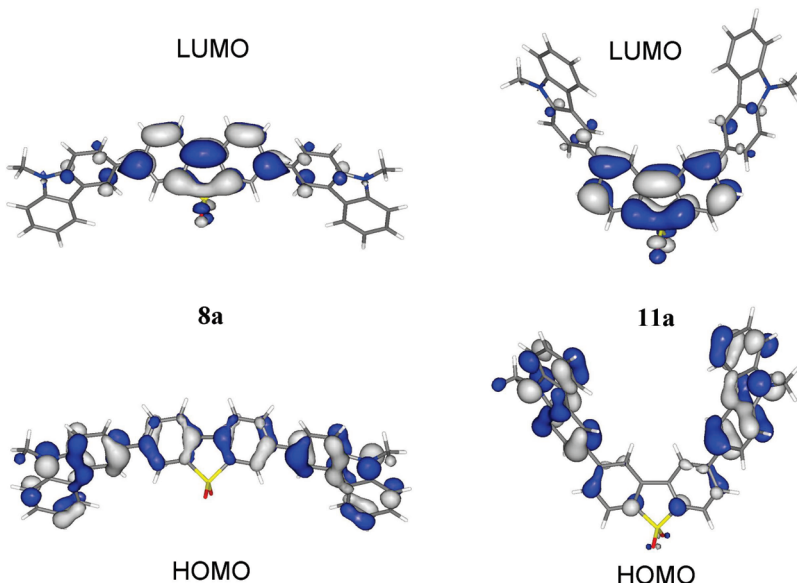


FIGURE 8. Frontier orbitals for **8a** and **11a**. Contour values are plotted at ± 0.03 (e/bohr^3) $^{1/2}$.

component is always below 2%, in agreement with the very small transient spectral relaxation observed in toluene, a low-polarity solvent. For compound **11**, and also for compound **1**,^{19b} additional time-resolved measurements were performed in ethanol, which is a solvent of high polarity (Figure 7). The decays collected in the high-energy region of the spectrum could be fitted with two exponential components with positive amplitudes. One component appears as a fast decay with a time constant of 28 ps, while the slower component has a time constant of 3.98 ns. The decays collected in the low-energy part of the spectrum could be fitted again with two exponential components. However, the amplitude of the fast one is now negative and its time constant is 23 ps, which correlates well with the time constant of the corresponding fast component of the high-energy region of the spectrum. The latter observation is a good indication that these components are due to the excited-state reorganization, controlled by solvent and molecular rearrangements, as observed for compound **1**.^{19b} The time constant of the slow component (3.93 ns) is also in excellent agreement with the corresponding one in the high-energy region of the spectrum. This indicates that the slow component is associated with the lifetime of the ICT state of this compound (**11**) in ethanol.

TABLE 5. Dihedral Angles between Donor (F, Cz, DPA, and TPA) and Acceptor (S) Units in Optimized Ground- (S_0) and Excited-State (S_1) Geometries and Energy Differences between These Geometries and Their Planar Forms

compd	S_0 dihedral (deg)	S_1 dihedral (deg)	$\Delta(S_0-S_1)$ dihedral (deg)	S_0 planar energy (kcal mol ⁻¹)	S_1 planar energy (kcal mol ⁻¹)
1a	38.3	22.0	16.3	3.9	2.5
8a	38.7	25.0	13.7	4.1	2.8
9a	39.6	31.8	7.8	5.5	4.4
11a	40.1	34.8	5.3	4.9	4.3
15a	38.3	23.6	14.7	4.3	3.0
17a	40.2	28.6	11.6	5.5	4.3
18a	40.7	27.6	13.1	4.8	3.2
20a	53.4	89.3	-35.9	25.9	24.0
21a	54.6	89.4	-34.8	27.9	25.6
23a	33.6	56.1	-22.5		
26a	35.6	17.7	17.9		

Ground-state (S_0) geometry optimizations were carried out on the 11 trimers at the B3LYP/6-311G** level of theory without symmetry constraints. Methyl groups were used instead of ethylhexyl or butyl groups (where present) to reduce computational efforts, and these model geometries are labeled with “a” for convenience. Many conformers were found, but no true minimum for a planar geometry was located in any trimer. Only the most stable conformers found are considered here, and their dihedral angles are listed in Table 5. Comparison of the geometrical parameters between the optimized model geometry **17a** and the experimental geometry^{21c} of **17** shows very good agreement. The dihedral angles between the F and S units are 40.2° in **17a** (theory) and between 36.7 and 46.0° in **17** (experimental).

Planar geometries were optimized using C_{2v} symmetry constraints (apart from **23a** and **26a**, where the tolyl groups at nitrogen would be unrealistically constrained to be perpendicular to the S unit) to obtain differences in energy between the planar and nonplanar geometries. These energy values are given in Table 5 and would be considered as rotational energy barriers to planar geometries. For the vast majority of the trimers, the energy barriers are in the range of only 4.0–5.5 kcal mol⁻¹. The donor and acceptor units are considered to be freely rotating in solution at ambient temperatures. The presence of fluorine atoms in **9a** and **17a** increases the energy barrier by only 1.4–1.6 kcal mol⁻¹ in comparison to **8a** and **1a**, respectively. The geometries of **20a** and **21a**, however, are computed to have considerably larger energy barriers at 25.9–27.9 kcal mol⁻¹. Planar geometries of **20a** and **21a** are unlikely to be present in solution at ambient temperatures, as hydrogens near the carbazolyl nitrogen severely hinder such planar geometries.

The singlet excited-state geometries (S_1) were also optimized without symmetry constraints and, like the ground-state geometries (S_0), nonplanar geometries were located as minima. The dihedral angles are smaller by 5–17° in all cases, except for **20a**, **21a**, and **23a**, where the angles are larger due to unfavorable steric factors involving the *N*-carbazolyl and **DPA** units. The S_1 planar geometries were also obtained using C_{2v} symmetry constraints and reveal slightly smaller energy barriers to planar forms in comparison to the ground-state geometries. The differences in the dihedral angles of 6.6–6.8° due to the fluorine atoms in **9** and **17** compared to **8** and **1** in the S_1 excited-state geometries indicate steric effects with the fluorine atoms but, as shown in their photophysical data and the small energy barriers to planar forms, these steric effects are not significant.

Molecular orbital calculations on the S_0 optimized geometries of the model trimers show that the HOMOs are located on the donor groups and LUMO on the S unit, in accord with

TABLE 6. Contributions (%) of the Donor and Acceptor Groups in the Frontier Orbitals

	LUMO		HOMO	
	acceptor	donor	acceptor	donor
1a	72	28	29	71
8a	84	16	22	78
9a	85	15	18	82
11a	90	10	13	87
15a	74	26	5	95
17a	76	24	23	77
18a	77	23	19	81
20a	93	7	16	84
21a	96	4	11	89
23a	86	14	36	64
26a	78	22	10	90

observed CV and photophysical data. The delocalized LUMOs suggest that the thiophene *S,S*-dioxide ring (rather than only the SO₂ unit) acts as the acceptor. The HOMO, LUMO, and HOMO–LUMO gap (HLG) energies are compared with the CV data in Table 1, where trends are clearly evident. The different absolute values are typical when comparing oxidation and reduction potentials with computed MO energies. The calculated HOMO energies correspond to the increasing electron-donating ability of the donor unit from fluorenyl (F) to carbazolyl (Cz) to arylamine groups (DPA, TPA). The calculated LUMO and HLG energies are also in broad agreement with observed reduction potentials and HLGs in Table 1.

The orbital contributions of the acceptor and donor units in the LUMO and HOMO for each trimer are shown in Table 6. When the linear and bent analogues of **8a** and **11a** are compared, it is clear that the HOMO and LUMO characters are more localized on the donor and acceptor units, respectively, for the bent isomers. These frontier orbitals are shown pictorially in Figure 8, where the HOMO and LUMO are considered as largely π (donor) and π^* (acceptor) orbitals, respectively, with more mixing in both orbitals for **8a**. Similar conclusions are found for the linear/bent pair, **1a** and **18a**. A slightly different scenario occurs for **20a** and **21a**, where the HOMO and LUMO compositions are similar in both cases and are essentially localized (Figure 9). This indicates that the conjugation present in other linear trimers is reduced in compound **20a**, due to significantly nonplanar orientations of the carbazolyl groups in **20a**.

TD-DFT computations were carried out on the S_0 model geometries to assign the nature of the transitions in the absorption spectra for the trimers, and the results are summarized in Table 7. In all cases, the observed lowest energy bands are π (donor) to π^* (acceptor) charge transfer transitions in nature. The charge transfer character of these transitions varies between 43% (**1a**) and 87% (**21a**). The bent trimers clearly have greater

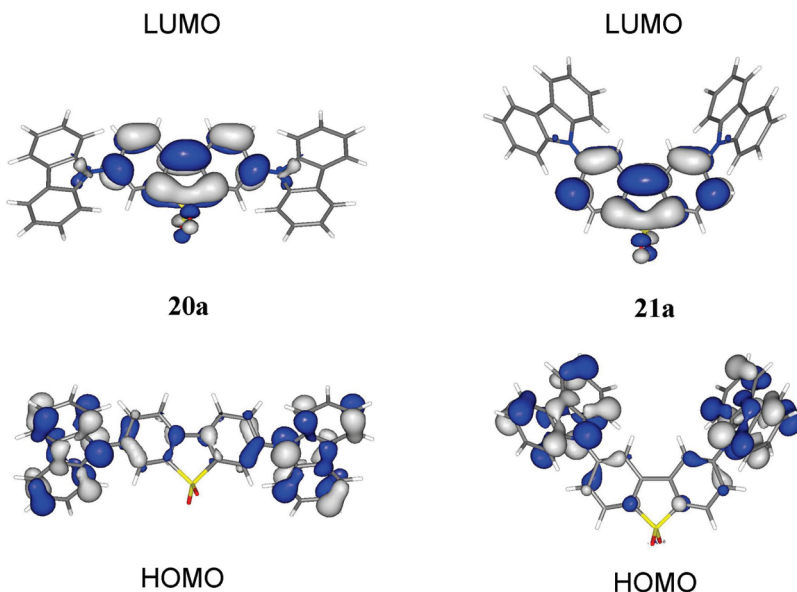


FIGURE 9. Frontier orbitals for **20a** and **21a**. Contour values are plotted at ± 0.03 (e/bohr^3) $^{1/2}$.

TABLE 7. Comparison of TD-DFT Data with Observed Absorption and Emission Data

	λ_{abs} (nm)			$\varepsilon (\text{M}^{-1} \text{cm}^{-1})$ obsd	transition type ^a	CT character (%)	λ_{em} (nm)	
	calcd	obsd	oscillation strength				calcd	obsd
1a	386	364	1.48	57 100	H > L	43	462	424
8a	391	379	0.98	34 900	H > L	62	458	443
9a	406	377	1.07	36 300	H > L	67	462	443
11a	298	299	0.11	62 800	H-4 > L ^c	30	406	408
	356	340	0.14	27 000	H-1 > L	81		
15a	331	339	0.21	38 800	H-2 > L+1	69	458	430
	384	370	0.81	53 000	H-2 > L	51		
17a	395	360	1.46	49 100	H > L	53	463	420
18a	321	300	0.24	47 000	H > L+1	56	405	382
	352	315	0.33	43 700	H > L	58		
20a	371	338	0.12	18 850	H > L+1	81	530	437
	425	377	0.41	14 760	H > L	77		
21a	360	333	0.12	13 000	H > L+1	87	516	424
	402	351 ^b	0.05	16 500	H-1 > L	84		
23a	316	298	0.27	20 600	H > L+4 ^d	29	545	482
	388	380	0.54	33 600	H > L+1	48		
	430	428 ^b	0.56	13 440	H > L	50		
26a	324	300	0.87	35 100	H-2 > L ^c	20	555	471
	456	411	1.21	40 500	H > L	68		

^aH = HOMO, L = LUMO. ^bShoulder. ^cLocal transition at S unit. ^dLocal transition at DPA units.

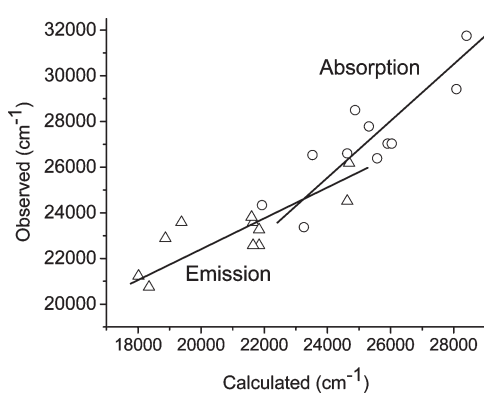


FIGURE 10. Correlation between observed and calculated absorption (circles) and emission (triangles) values.

CT character than their linear analogues (**8a** vs **11a**, **1a** vs **18a**), which is reflected in their photophysical properties. In the absorption spectra for **11**, **23**, and **26**, there are distinct, strong bands at around 300 nm which are assigned as local π to π^* transitions on the basis of TD-DFT data. Calculated emission data were obtained from TD-DFT computations on S_1 optimized geometries. The emission values listed in Table 7 correspond to the lowest energy transition in each case and are assumed to be π^* (acceptor) to π (donor) charge transfer transitions. Figure 10 shows reasonable correlations between observed and computed values for both absorption and emission data, where absolute values of observed and computed data are typically different.

Conclusions

Donor–acceptor–donor S-based oligomers have been synthesized where the donor strength has been increased in

the series fluorene → carbazole → arylamine. Their photochemical properties have been investigated in detail, with particular emphasis on probing the charge transfer character of the singlet excited state. The substitution of fluorene by carbazole red-shifts the emission from deep blue to sky blue. For the arylamine analogues the emission is further red-shifted into the green region. We have also investigated the effect of conjugation between the donor and acceptor units and demonstrated that the para versus meta conjugation between the successive phenyl rings controls the properties having a strong effect on the ICT character and emission yield of the singlet excited state. These results demonstrate a promising strategy for exploiting ICT states in ambipolar oligomers to tune the emission across the deep blue–green spectral region while retaining moderate to high photoluminescence quantum yields. Furthermore, a number of these oligomers have the potential to be developed into polymers for use as emissive materials in optoelectronic devices. The high stability of fluorene, carbazole, and dibenzothiophene *S,S*-dioxide derivatives is very attractive in this regard.

Experimental Section

General Procedure: Palladium-Catalyzed Cross-Coupling. 3,7-Dibromodibenzothiophene *S,S*-dioxide (**6**) or 2,8-dibromodibenzothiophene *S,S*-dioxide (**10**) (1 equiv) and the boronic

acid derivative **5**, **14**, or **16** (2.2 equiv) were dissolved in 1,4-dioxane or toluene. The solution was degassed by bubbling argon through it for 15 min. Dichlorobis(triphenylphosphine)-palladium(II) (3–5 mol %) or tetrakis(triphenylphosphine)-palladium(0) (5 mol %) was added and the solution degassed further. Degassed potassium carbonate solution (2 M) or degassed sodium carbonate (1 M) was added under argon and the solution heated to 110 °C for 24 h with protection from sunlight. The resulting slurry was poured into aqueous sodium chloride solution (5%), and the organic product was extracted into dichloromethane (DCM). The organic layer was washed with water until pH 7 and dried over magnesium sulfate ($MgSO_4$). After removal of the solvent under vacuum, the residue was purified by column chromatography to obtain the product.

Acknowledgment. This work was carried out as part of the TSB-funded TOPLESS project. We thank Dr. G. Williams (Zumtobel LED Division) for supporting this work, Durham University for funding (K.C.M.) and for access to its High Performance Computing facility. We thank the Royal Society for funding (V.B.).

Supporting Information Available: Text, figures, and tables giving details of experimental procedures, characterization data, absorption and fluorescence spectra, fluorescence decays, solution electrochemical data, and computations. This material is available free of charge via the Internet at <http://pubs.acs.org>.